Ecological Modelling 451 (2021) 109567

Contents lists available at ScienceDirect

Ecological Modelling

journal homepage: www.elsevier.com/locate/ecolmodel

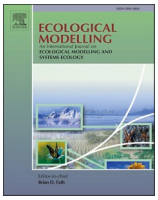

Microclimc: A mechanistic model of above, below and within-canopy microclimate

Ilya M.D. Maclean, Writing – Original Draft Preparation; Writing – Review & Editing [a,*], David H. Klinges, Validation; Writing – Original Draft Preparation; Writing – Review & Editing [b,c]

[a] Environment and Sustainability Institute, University of Exeter Penryn Campus, Penryn, United Kingdom, TR13 9FG
[b] School of Natural Resources and Environment, University of Florida, Gainesville, FL, United States
[c] Smithsonian Environmental Research Center, Edgewater, MD, United States

ARTICLE INFO

Keywords:
Temperature
Climate
Mechanistic model
Biophysical ecology
Evapotranspiration
R package

ABSTRACT

Climate strongly influences ecological patterns and processes at scales ranging from local to global. Studies of ecological responses to climate usually rely on data derived from weather stations, where temperature and humidity may differ substantially from that in the microenvironments in which organisms reside. To help remedy this, we present a model that leverages first principles physics to predict microclimate above, within, and below the canopy in any terrestrial location on earth, made freely available as an R software package. The model can be run in one of two modes. In the first, heat and vapour exchange within and below canopy are modelled as transient processes, thus accounting for fine temporal-resolution changes. In the second, steady-state conditions are assumed, enabling conditions at hourly intervals or longer to be estimated with greater computational efficiency. We validated both modes of the model with empirical below-canopy thermal measurements from several locations globally, resulting in hourly predictions with mean absolute error of 2.77 °C and 2.79 °C for the transient and steady-state modes respectively. Alongside the microclimate model, several functions are provided to assist data assimilation, as well as different parameterizations to capture a variety of habitats, allowing flexible application even when little is known about the study location. The model's modular design in a programming language familiar to ecological researchers provides easy access to the modelling of site-specific climate forcing, in an attempt to more closely unify the fields of micrometeorology and ecology.

1. Introduction

Temperature and water availability influence almost every ecological pattern and process, from the chemical reactions that control photosynthesis (Ingenhousz et al., 1779; Kumarathunge et al., 2019), to the global distribution of biomes (Gardner et al., 2020; Geiger, 1954; Köppen, 1884). Over the last two centuries thousands of ecological studies have investigated relationships between organisms and climate and one of the great challenges in modern ecology is to predict responses to climate change. A common feature of many of these studies is that the climate data used are derived or modelled from weather station data (Bramer et al., 2018; Potter et al., 2013). The microclimatic conditions experienced by organisms can differ vastly from the conditions ~1.5 m above the ground, measured inside a weather station screen (Maclean et al., 2019; Suggitt et al., 2011). Consequently, meteorological data will often incorrectly predict physical exposure to critical climate thresholds and the timing of climate-sensitive biological events (Baker, 1980; Perez and Feeley 2020). Microclimatic conditions in low-lying vegetation are also far more spatially and temporally variable than inside weather stations (Bennie et al., 2008; Lenoir et al., 2017), implying that the climatic niches of species, fundamental to predicting their distributions changes, cannot be accurately established by the methods normally used. Neglecting this variability, which can provide microrefugia or allow for thermoregulation, can also lead to overestimation of extinction rates (Suggitt et al., 2018). There is thus a clear need to develop methods that estimate microclimatic conditions of the environments in which organisms reside.

In fields outside ecology, the modelling of microclimates has a long history. Many of the methods used still owe their origins to the pioneering work by Richardson (1922), who demonstrated the basic laws of turbulent mixing in the surface layer of the atmosphere. In the 1950s, Monin and Obukhov (1954), extended this platform and, building on

* Corresponding author.
E-mail address: i.m.d.maclean@exeter.ac.uk (I.M.D. Maclean).

https://doi.org/10.1016/j.ecolmodel.2021.109567
Received 9 November 2020; Received in revised form 4 March 2021; Accepted 1 April 2021
Available online 3 May 2021

work by Prandtl (1925), provided a generalised, universal method for characterising wind speed and temperature profiles above the surface of a vegetation canopy under non-neutral conditions. The methods developed by these earlier pioneers in microclimatology still form the basis of most models that are in use today (see e.g. Ali et al., 2018; Bruse, 2014). Ecologists, however, have been surprisingly slow to adopt these more mechanistic approaches, and there is a still a tendency to derive microclimatic surfaces using statistical approaches (Fick and Hijmans, 2017; Greiser et al., 2018; Meineri and Hylander, 2017). While potentially very good at capturing spatial variation in microclimate, the potential for models fitted using statistical inference to forecast novel conditions is somewhat questionable (Buckley et al., 2018; Evans, 2012; Nabi, 1985).

Nevertheless, the last few years have witnessed renewed ecological interest in microclimatology (Bramer et al., 2018; Lembrechts et al., 2019; Potter et al., 2013), in part driven by the availability of models written using programming languages with which ecologists are familiar (Lembrechts and Lenoir, 2019). One of the most widely used microclimate models in ecology, that of Porter et al. (1973), has been incorporated into the R package 'NicheMapR' (Kearney and Porter, 2017). Although flexible and widely tested, it requires pre-adjustment of input forcing to account for terrain and canopy shading effects as well as mesoclimatic processes such elevation and cold air drainage. It is also designed to be run for single point locations. Building on the model of Bennie et al. (2008), Maclean et al. (2017) developed methods for modelling mesoclimatic effects, released as an R-package 'microclima', which is able to produce gridded estimates of microclimate (Maclean et al., 2019). Both models have subsequently been combined into a single framework (Kearney et al., 2020) and have also been developed for application in forecasting future climate (Maclean, 2020). Importantly, however, they were designed primarily for modelling above-canopy microclimate, and have principally been applied to determine microclimatic conditions over short vegetation. The environmental physics underpinning the models are associated with exchange above a vegetated surface and do not explicitly consider the microclimate within canopies. However, tropical forests alone host at least two-thirds of the worlds terrestrial biodiversity (Gardner et al., 2009), and with the exception of soil biota, the majority of remaining species spend at least some of their time amongst vegetated canopies (Lowman et al., 1996; Nakamura et al., 2017). In addition, thermal tolerances of plants are more sensitive to leaf temperatures than ambient air temperatures (Michaletz et al., 2016; Perez and Feeley 2020) and critical thermal thresholds can vary even within the canopy of a single tree (Curtis et al., 2019). Means of determining the microclimatic conditions across and below the canopy are therefore much needed.

In contrast to above the canopy, however, the physics of microclimate below-canopy is not fully resolved. Above-canopy, the transport of heat and vapour can accurately be described from estimates of atmospheric turbulence using *K*-theory (i.e. using a flux gradient approach). Emerging understanding (see e.g. Baneree et al., 2017), suggests that *K*-theory often fails to describe turbulent transport in plant canopies. Many of its assumptions are violated because within-canopy air turbulence is an intermittent process: infrequent wind gusts sweeping downward through the trunk space from the air above are responsible for much of the exchange of heat, vapour and momentum between the canopy and the atmosphere. The 'effective diffusivity' of heat and vapour is more often a function of the vertical distribution of heat and water vapour sources or sinks within the canopy than of the turbulence level. Simulation of within-canopy turbulence is thus improved upon by using Lagrangian (e.g. Raupach, 1989) or Eulerian (e.g. Katul and Albertson, 1999) advection-diffusion models. The utility of such models for ecological applications, however, is severely limited by their need to specify length and time scales for the wind field. *K*-theory models are least valid when they are used to estimate within-canopy water vapour and heat exchange, but it is by virtue of this fact that it is still possible to simulate realistic in-canopy microclimates using *K*-theory. This apparent inconsistency arises for two reasons. First, although the source-sink strengths and hence the distribution of heat and momentum fluxes are extremely sensitive to the shape of measured profiles (Finnigan, 2000; Raupach and Thom, 1981), the converse relationship means that shape of the temperature and wind profiles are insensitive to flux uncertainties and can be generated by integration of an appropriate distribution of sources. Second, both temperature and humidity are related strongly to latent heat fluxes, which in turn are more strongly controlled by stomatal conductance than by turbulence within the canopy (Jarvis and McNaughton, 1986). In consequence, a realistic representation of the distribution of foliage density, net radiation and stomatal conductance in various layers of a canopy, coupled with a relatively uncertain model of atmospheric transfer within the canopy, will tend to adequately reproduce temperature, vapour and wind profiles (Monteith and Unsworth, 2013).

Thus, despite evolving views of the processes driving turbulence within plant canopies, different models developed over several decades (e.g. Bailey et al., 2016; Baldocchi and Meyers, 1998; Goudriaan, 1977; McNaughton and Van den Hurk, 1995; Waggoner et al., 1969) have all used a similar approach. First, the vertical distribution of radiant energy within the canopy is quantified from foliage density and radiation transmission. Second, the net radiation absorbed by each leaf is divided up into sensible and latent heat, making appropriate assumptions about stomatal and leaf boundary layer conductance. Last, the transfer of air within different layers of the canopy is modelled using a variety of different approaches (e.g. *K*-theory, Langrangian or Eularian models) and have all been shown to perform in a similar fashion and relatively well (Bache, 1986; Dolman and Wallace, 1991). Nevertheless, a practical, 'off-the-shelf' model that can be used by ecologists to estimate microclimate conditions is still lacking.

Here we develop an integrated above/below-canopy and soil microclimate model, in the R programming environment, for application in ecological research. The model, based on first principles physics, is designed to be flexible, enabling application in almost any terrestrial environment though its intended focus is primarily to estimate within-canopy temperatures. Through its modular design, and careful selection of vegetation parameters typical of a given vegetation derived from literature, it can be applied with little knowledge of the particular study location (as a minimum, just a user-specified broad habitat type). However, the option to alter parameters (for example, stomatal conductance, or leaf area at varying heights in the canopy) is included to enable more complex, bespoke parametrisations where possible. The model can also be run using freely available climate data using tools that we have previously developed for downloading (Duffy, 2020; Kearney et al., 2020).

2. Model description

2.1. Overall model structure

The model is designed to be run at single-point locations, using a time-series of climate forcing data (temperature, humidity, wind speed, atmospheric pressure and incoming solar radiation). It can be run in two modes at time-increments ranging from seconds to days. For application where very fine-temporal resolution data might be needed, heat and vapour exchange are modelled as transient processes, and heat storage by the canopy, and the exchange of heat between different layers of the canopy, are considered explicitly, with the capacity to simulate wind gusts thus bi-passing limitations associated with *K*-theory. Alternatively, for application at time increments of an hour or longer, below-canopy heat and vapour exchange are assumed to attain steady state, and the temperatures and soil moisture are determined using energy balance equations that sum to zero. In this latter mode, the model has been integrated with `NicheMapR` package (Kearney and Porter, 2017) and uses the rapid processing capacity of Fortran routines therein to compute soil moisture and temperature. It also enables explicit

modelling of snow.

In the transient mode, the canopy and soil profiles are divided into a user-specified number of layers (with a default of 20). For each layer, the user specifies canopy properties (e.g. leaf area, leaf angle distribution, leaf reflectance and maximum stomatal conductance) and soil (e.g. bulk density, mineral, organic, quartz and clay content, Campbell 1985), or alternatively these are estimated for each layer by specifying habitat or soil type or providing single values for the entire canopy and soil profile. In the steady-state mode, the user specifies a height below ground or above/within the canopy, and the leaf area above this point and for the canopy in total must be specified (although the option to estimate these by specifying a habitat type is also included). In both modes, above-canopy temperature, humidity and wind profiles are calculated using *K*-theory with estimates of bulk aerodynamic resistance derived from canopy properties. Within the canopy, radiation transmission and wind profiles are also estimated from canopy properties. These, in turn, are used to estimate turbulent transfer within the canopy and boundary layer and stomatal conductance for each canopy layer. Heat balance equations for each canopy layer are then linearized, enabling simultaneous calculation of leaf and air temperatures. Time-dependant differential equations for each canopy and soil node are then specified and storage and simultaneous exchanges of heat and vapour between each layer then computed. In the transient mode, storage is considered both for soil and the canopy, but in the steady-state mode, only storage in the soil is considered. The model returns a time-series of temperature, humidity and wind speeds at user-specified heights or depths.

Below we provide a general overview of the equations used in the model. All symbols and their units are described in Table 1, and further details of these equations and their derivation are provided in Appendix A.

2.2. Solar radiation

Radiation is the key source of heat within a canopy and has a major bearing on rates of evapotranspiration. The net radiation flux is determined by the balance of incoming shortwave radiation and emitted longwave radiation, a portion of the latter of which is also absorbed by leaves. Direct radiation is partitioned into direct (beam) and diffuse components, both of which are attenuated by the canopy. Following Campbell (1986) and Campbell & Norman (2012), the flux density of beam radiation $R_b^{P_{AI}}$ under plant area P_{AI} is described as follows:

$$R_b^{P_{AI}} = R_b^0\left\{(1-\Omega)\exp\left(-\sqrt{1-r_s}\,KP_{AI}\left(\frac{1}{1-\Omega}\right)\right)+\Omega\right\} \quad (1a)$$

where R_b^0 is the flux density of beam radiation on a horizontal surface above the canopy, r_s is the reflectance of leaves to shortwave radiation, Ω (scaled between 0 and 1) describes how clumped the canopy is such that some radiation passes directly though canopy gaps. *K*, the extinction coefficient of light, represents the area of shadow cast on a horizontal surface by the canopy divided by the plant area of the canopy, and depends on the ratio of vertical to horizontal projections of a representative volume of foliage, *x*:

$$K = \frac{\sqrt{x^2+\tan^2 Z}}{1.774(x+1.182)^{-0.733}}$$

where *Z* is the solar zenith angle. For diffuse radiation, the leaf angle distribution is unimportant, and (1a) becomes

$$R_d^{P_{AI}} = R_d^0\left\{(1-\Omega)\exp\left(-\sqrt{1-r_s}\,P_{AI}\left(\frac{1}{1-\Omega}\right)\right)+\Omega\right\} \quad (1b)$$

where R_d^0 is the flux density of diffuse radiation above the canopy, $R_d^{P_{AI}}$ is the flux density of below plant area P_{AI}. The temperature of leaves is dependant on the amount of radiation absorbed. Assuming the canopy to be made up of *n* layers, each with a plant area, $P_{AI}[i]$, such that P_{AI}

Table 1
List of symbols used in equations.

Term	Definition	Units
a	Wind attenuation coefficient	–
b	Exponent for water release from soil	–
c_d	Drag coefficient	–
C_D	Volumetric specific heat capacity of vegetation	$J\bullet m^{-3}\bullet K^{-1}$
C_H	Volumetric specific heat capacity of soil	$J\bullet m^{-3}\bullet K^{-1}$
c_p	Specific heat of air at constant pressure	$J\bullet mol^{-1}\bullet K^{-1}$
d	Zero plane displacement	m
D_H	Thermal diffusivity	$m^2\bullet s^{-1}$
e	Vapour pressure	Pa
e_L	Vapour pressure of leaf	Pa
e_s	Saturated vapour pressure	Pa
E	Evaporation rate of water	$mol\bullet m^{-2}\bullet s^{-1}$
g	Molar conductance	$mol\bullet m^{-2}\bullet s^{-1}$
g_c	Stomatal conductance	$mol\bullet m^{-2}\bullet s^{-1}$
g_{cmx}	Maximum stomatal conductance	$mol\bullet m^{-2}\bullet s^{-1}$
g_{Ha}	Leaf boundary layer conductance for heat	$mol\bullet m^{-2}\bullet s^{-1}$
G_r	Grashof number	–
g_v	Leaf conductance for vapour	$mol\bullet m^{-2}\bullet s^{-1}$
g_t	Conductance for heat by turbulent transfer	$mol\bullet m^{-2}\bullet s^{-1}$
h	Canopy height	m
H	Sensible heat flux density	$W\bullet m^{-2}$
i_w	Relative turbulence intensity	–
l_m	Mixing length	m
l_{tr}	Transmission fraction of longwave radiation through the canopy	–
k	Thermal conductivity	$W\bullet m^{-1}\bullet K^{-1}$
K	Extinction coefficient for canopy radiation transmission	–
m_i	Ratio of radiation incident on inclined leaves in each canopy layer relative to the horizontal	–
n	Thomas algorithm forward-backward weighting factor	–
p_a	Atmospheric pressure	Pa
p_s	Fraction of sunlit leaves	–
P_{AI}	Plant area index	–
P_r	Prandtl number	–
P_v	Fractional foliage volume	–
Q_a	Photosynthetically active radiation absorbed by a leaf	$mol\bullet m^{-2}\ s^{-1}$
Q_{a50}	Value of Q_a when g_v is at 50% of maximum	$mol\bullet m^{-2}\ s^{-1}$
R_{abs}	Total radiation absorbed by canopy layer	$W\bullet m^{-2}$
R_{em}	Total radiation emitted by canopy layer	$W\bullet m^{-2}$
R_b^0	Flux density of beam radiation on a horizontal surface above the canopy	$W\bullet m^{-2}$
$R_b^{P_{AI}}$	Flux density of beam radiation below plant area P_{AI}	$W\bullet m^{-2}$
R_d^0	Flux density of diffuse radiation above the canopy	$W\bullet m^{-2}$
$R_d^{P_{AI}}$	Flux density of diffuse radiation below plant area P_{AI}	$W\bullet m^{-2}$
R_e	Reynolds number	–
r_l	Leaf reflectivity (longwave radiation)	–
R_l^{abs}	Longwave radiation absorbed by canopy layer	$W\bullet m^{-2}$
R_l^{can}	Longwave radiation emitted by canopy to each layer	$W\bullet m^{-2}$
R_l^{em}	Emitted longwave radiation	$W\bullet m^{-2}$
R_l^{sky}	Longwave radiation emitted by sky	$W\bullet m^{-2}$
r_s	Leaf reflectivity (shortwave radiation)	–
R_s^{abs}	Shortwave radiation absorbed by canopy layer	$W\bullet m^{-2}$
R_s^{PAI}	Flux density of shortwave radiation below plant area P_{AI}	$W\bullet m^{-2}$
t	Time step	s
T_{d+z_H}	Temperature at heat exchange surface of canopy	K
T_j	Temperature at time j	K
T_z	Temperature at height z	K
T_L	Leaf temperature	K
u^*	Friction velocity of wind	$m\bullet s^{-1}$
u_h	Wind speed at top of canopy	$m\bullet s^{-1}$
u_z	Wind speed at height z	$m\bullet s^{-1}$
V_d	Volumetric density of vegetation	$kg\bullet m^{-3}$

(*continued on next page*)

Table 1 (*continued*)

Term	Definition	Units
w	Mean leaf width	m
x	Ratio of vertical to horizontal projections of a representative volume of foliage	
x_d	Characteristic dimension of leaf	m
z	Height	m
Z	Solar zenith angle	°
z_H	Roughness length for heat	m
z_{LA}	Mean leaf-air distance	m
z_M	Roughness length for momentum	m
λ	Latent heat of vaporization of water	J•mol^{-1}
θ	Volumetric soil moisture fraction	–
θ_s	Saturated volumetric soil moisture fraction	–
$\widehat{\rho}$	Molar density of air	mol•m^{-3}
σ	Stefan-Boltzman constant	W•m^{-2}•K^{-4}
ψ_e	Air entry water potential	J•kg^{-1}
ψ_H	Diabatic correction for heat	–
ψ_M	Diabatic correction for momentum	–
Ω	Canopy clumping factor	–

represents the plant area above any given layer, then the flux density of solar radiation absorbed (R_s^{abs}) by each layer is

$$R_s^{abs} = P_{AI}[i](1-r_s)\left(p_s m_i R_s^{PAI} + (1-p_s)R_s^{PAI}\right) \quad (2)$$

where R_s^{PAI} is the flux density of solar radiation below plant area P_{AI} given by $R_b^{P_{AI}}+R_d^{P_{AI}}$ and p_s is the fraction of sunlit leaves given by

$$p_s = (1-\Omega)\left(\frac{1-\exp\left(-KP_{AI}\frac{1}{1-\Omega}\right)}{P_{AI}K}\right)+\Omega$$

and m_i is the ratio of radiation incident on inclined leaves in each canopy layer relative to the horizontal, which from Campbell (1990) is approximated as follows:

$$m_i = \exp\left\{1.206x^{0.407} - 4.89 - \left(0.412x^{0.317}+1.324\right)\log(90-Z)\right\}^{-1}$$

2.3. Longwave radiation

From the Stefan–Boltzman law, the flux density of longwave radiation emitted by vegetation, R_l^{em}, with plant area $P_{AI}[i]$ is

$$R_l^{em} = P_{AI}[i](1-r_l)\sigma {T_L}^4 \quad (2a)$$

where r_l is reflectance to longwave radiation, σ is the Stefan-Boltzman constant and T_L is the temperature of the leaf. A portion of emitted radiation is then reabsorbed. The absorbed longwave radiation, R_l^{abs}, depends on sky emissivity and upwards and downwards transmission through the canopy

$$R_l^{abs} = P_{AI}[i](1-r_l)\left(R_l^{sky}+R_l^{can}\right) \quad (2b)$$

where R_l^{sky} is longwave radiation absorbed and re-emitted downward from the sky, given by $R_l^{sky} = \varepsilon_s(l_{tr})^2 R_l^{em}$ and R_l^{can} is radiation absorbed and re-emitted downward from the canopy, given by $R_l^{can} = (1-l_{tr})R_l^{em}$, where ε_s is sky emissivity and l_{tr} is transmission of longwave radiation through the canopy given by $l_{tr} = (1-\Omega)\exp\left(-\sqrt{1-r_l}P_{AI}\left(\frac{1}{1-\Omega}\right)\right)+\Omega$.

2.4. Wind, conductance and temperature above-canopy

Wind profiles above the canopy dictate heat and vapour exchange between the canopy and air above it, and therefore ultimately determine temperature and vapour profiles. It can generally be assumed that radiative fluxes have a negligible effect on air temperature directly. However, the canopy itself acts as a heat exchange surface, enabling exchange of heat with surrounding air via a process of eddy diffusion. Following Campbell and Norman (2012) the wind profile is describe as follows:

$$u_z = \frac{u^*}{0.4}\ln\frac{z-d}{z_M}+\psi_M \quad (3)$$

where u_z is wind speed at height z, d is the height above ground within the canopy where the wind profile extrapolates to zero, z_m the roughness length for momentum, ψ_M is a diabatic correction for momentum (see Appendix A) and u^* is the friction velocity, which gives the wind speed at height $d+z_m$.

The equation that describes the temperature profile is given as follows:

$$T_z = T_{d+z_H} - \frac{H}{0.4\widehat{\rho}c_p u^*}\left(\ln\frac{z-d}{z_H}+\psi_H\right) \quad (4)$$

where T_z is temperature at height z, T_{d+z_H} is the temperature at the height of the exchange surface $d+z_H$, z_H is the roughness length for heat transfer, ψ_H the diabatic correction for heat and $\widehat{\rho}$ and c_p the specific heat and molar density of air respectively. The sensible heat flux H is, in effect, the net heat supplied to the canopy surface as determined from the balance of radiative, latent and ground heat fluxes. Coefficients d, z_M and z_H can be derived through empirical measurement of temperature and wind profiles, but the model includes more general expressions of these derived by Shaw and Pereira (1982) as functions P_{AI} and canopy height (h). The diabatic correction factors account for the fact that strong surface heating causes overturning of the air layers, with resultant increases in turbulence and mixing and vis-versa. Further details of how these are calculated are provided in Appendix A.

Heat conductance, g_t (mol•m^{-2}•s^{-1}) between any two heights z_1 and z_0 above-canopy, expressed in molar form is then given by

$$g_t = \frac{0.4\widehat{\rho}u^*}{\ln\left(\frac{z_1-d}{z_0-d}\right)+\psi_H} \quad (5)$$

2.5. Wind, and heat conductance below-canopy

From Inoue (1963), Cionco (1972) and Goudriaan (1977), a wind profile within the canopy can be derived as follows:

$$u_z = u_h\exp\left(a\left(\frac{z}{h}-1\right)\right) \quad (6)$$

where u_z is wind speed at height z within the canopy, u_h is wind speed at the top of the canopy at height h, and a is a wind attenuation coefficient given by $a = \frac{c_d P_{AI} h}{2 l_m i_w}$, where c_d is a drag coefficient that varies with leaf inclination and shape, i_w is a coefficient describing relative turbulence intensity and l_m is the mean mixing length, equivalent to the free space between the leaves and stems. From Goudriaan (1977) $l_m = \sqrt{\frac{4wh}{\pi P_{AI}}}$, for vegetation that is long and narrow, or $l_m = \sqrt[3]{\frac{6w^2h}{\pi P_{AI}}}$ for leaves shaped more like squares, where w is the mean width of leaves and stems. Within-canopy heat conductance between any two heights z_1 and z_0 below-canopy is then given by

$$g_t = \frac{u_h l_m i_w a}{\left(\exp\left(\frac{-az_0}{h-1}\right)-\exp\left(\frac{-az_1}{h-1}\right)\right)\psi_H} \quad (7)$$

where ψ_H is a within-canopy diabatic correction factor for heat (see Appendix A). It is also necessary to calculate conductance, g_{Ha}, between the leaf and air. When wind speeds are moderate to high, conduction is

predominantly under laminar forced convection and from e.g. Campbell and Norman (2012) is given by

$$g_{Ha} = \frac{0.664\widehat{\rho}D_H R_e^{0.5} P_r^{0.5}}{x_d} \quad (8a)$$

where D_H is thermal diffusivity, x_d is the characteristic dimension of the leaf ($x_d \approx 0.7w$), R_e is the Reynolds number, and P_r is the Prandtl number. When wind speeds are low, an expression that is adequate for leaves is given by (Campbell and Norman, 2012)

$$g_{Ha} = \frac{0.54\widehat{\rho}D_H (G_r P_r)^{0.25}}{x_d} \quad (8b)$$

where G_r is the Grashof number. When the leaf is cooler than the air, the heat transfer is only half as efficient so the constant 0.54 becomes 0.26. Equations (8a & b) describe conductance one would measure under minimal turbulence. Based on measurements by Mitchell (1976), and following Campbell and Norman (2012), turbulence is accounted for by using an enhancement factor of 1.4. Formulae for computing the Reynolds, Prandtl and Grashof numbers are provided in Appendix A.

2.6. Vapour and latent heat fluxes

Vapour gradients control both evapotranspiration rates and latent heat fluxes and thus have a significant bearing on temperature and humidity. From Fick's law, the transport of vapour is given by

$$\lambda E = g\frac{\partial e}{p_a} \quad (10)$$

where λE is latent heat, comprising the latent heat of vapourization of water (λ) and the evaporation rate (E), ∂e is the vapour pressure gradient and p_a is atmospheric pressure. For vapour exchange above the canopy or between layers of air within the canopy, the conductance is the same as that for heat. The conductance for vapour loss from leaves (g_v), however, also depends on stomatal conductance (g_c)

$$g_v = 1/(1/g_{Ha} + 1/g_c)$$

Under ample root water supply, non-extreme temperatures and low humidity deficit, $g_c$varies through the canopy only in response to variation in photosynthetically active radiation. The stomatal response to the photosynthetically active radiation by an individual leaf (Q_l), can be assumed (Kelliher et al., 1995) to be given by a hyperbolic function:

$$g_c = \frac{Q_a}{Q_a + Q_{a50}} g_{cmx} \quad (11)$$

where g_{cmx} is maximum stomatal conductance and Q_{a50} is the value of Q_a when $g_v = g_{vmx}/2$. Körner (1995) gives values of g_{cmx} for most major vegetation types in the world.

It can generally be assumed that the water potential of leaves is such that vapour concentration at the evaporating surface is equal to the saturated vapour concentration at surface temperature, such that e_s can be determined from leaf temperature (T_L). For the soil surface, an equivalent to vapour pressure can, from Campbell and Norman (2012), be calculated as $e_a = e_s \exp((\theta/\theta_s)^{-b}(0.018\psi_e/8.31T_0))$, where e_s is calculated using soil surface temperature (T_0), θ is soil volumetric water content, θ_s the saturated water content, ψ_e the air entry water potential and b the exponent for water release. The parameters θ_s, ψ_e and b depend on soil type, but are otherwise constant.

2.7. Below-canopy temperature and humidity

Under steady-state, the heat balance equation for the leaves in each canopy layer is as follows:

$$\overline{R}_{abs} - \overline{R}_{em} - \overline{H} - \overline{\lambda E} = \overline{R}_{abs} - \varepsilon_s \sigma \overline{T}_L^{\,4} - c_p \overline{g}_{Ha}\left(\overline{T}_L - \overline{T}_A\right) - \lambda \overline{g}_v \frac{e_L - \overline{e}_A}{\overline{p}_a} = 0 \quad (12)$$

Where $\overline{R}_{abs}$ is absorbed radiation, $\overline{R}_{em}$emitted radiation, $\overline{H}$ the sensible heat flux, $\overline{\lambda E}$ the latent heat flux, ε_s the emissivity of the leaf, σ the Stefan-Boltzmann constant, $\overline{T}_L$ the absolute temperature of the leaf, $\overline{T}_A$ the absolute temperature of the air surrounding the leaf, λ the latent heat of vaporisation of water, e_L the effective vapour pressure of the leaf, $\overline{e}_a$ the vapour pressure of air and $\overline{p}_a$ atmospheric pressure. Throughout, overbars denote a mean over the duration of the time-step.

A challenge in solving this equation is the dependency of latent heat and emitted radiation on leaf temperature. The emitted radiation term can be solved readily by linearisation using binomial expansion (see Appendix A). The latent heat term is usually solved algebraically through linearization using the Penman-Monteith equation (Monteith, 1965; Penman, 1948), by assuming that air temperature surrounding a leaf is closely coupled to the air above and uninfluenced by leaf temperature. We explicitly consider the effects of leaf temperature on air temperature, and also the degree of coupling with the soil and air above canopy. Defining a term, ΔT_L, such that $T_L = T_A - \Delta T_L$ and a linear expression for air temperature such that $T_A = a_A + b_A \Delta T_L$, it can be shown (see Appendix A) that

$$\Delta T_L = \frac{R_{abs} - a_R - a_L}{1 + b_R + b_L + b_H}$$

Where equations for each a and b term are provided in Table 2. Under transient conditions the heat storage of each canopy layer is sufficient to prevent equilibrium. If superscript j denotes present time, and $j+1$ is one time-step in the future it can reasonably be assumed that e.g. $\overline{T} = 0.5(T^j + T^{j+1})$. Defining m_L as the flux density required to heat a m^3 of vegetation by one degree K, given by $z_{LA} C_d V_d / t P_{AI}$, where z_{LA} is the mean leaf-air distance (equivalent to half the average distance between leaves), C_d the specific heat capacity of vegetation with volumetric density V_d, t the duration of each model time step and P_{AI} the total one-sided plant area per m^2 ground area, an equivalent expression for the transient leaf temperature change is given as follows:

$$T_L^{j+1} = T_L^j + \frac{\overline{R}_{abs} - a_R - a_H - a_L}{m_L(1 + b_R + b_H + b_L)} \quad (13)$$

Expressions for each a and b under transient conditions are also given in Table 2 and derivation of the equation is in Appendix A.

2.8. Soil temperature

In the soil, heat storage is almost always significant, and Fourier's Law is combined with the continuity equation to obtain a time dependant differential equation that describes soil temperature as a function of depth and time: $C_h \partial T/\partial t = \partial(k \partial T/\partial z)\partial z$, where C_h is volumetric specific heat and k thermal conductivity in $W \bullet m^{-1} \bullet K^{-1}$ ($k = c_p \partial z g$), determined from soil properties and volumetric water content (Appendix A). A closed-form solution to this time-dependant differential equation that extends beyond simple sets of soil properties and boundary conditions is not possible. Following Campbell (1985), a numerical solution is achieved by dividing the soil into layers. Each layer is assigned a node, i, at depth, z_i, and with heat storage, Ch_i, and nodes are numbered sequentially downward such that node $i+1$ represents the node for the soil layer immediately below. Conductivity, k_i, represents conductivity between nodes i and $i+1$. The energy balance equation for node i is then given by

$$\overline{\kappa}_i\left(\overline{T}_{i+1} - \overline{T}_i\right) - \overline{\kappa}_{i-1}\left(\overline{T}_i - \overline{T}_{i-1}\right) = \frac{C_{h_i}\left(T_i^{j+1} - T_i^j\right)(z_{i+1} - z_{i-1})}{2\Delta t} \quad (14)$$

where Δt is the time increment, conductance, $\kappa_i = k_i/(z_{i+1} - z_i)$, su-

Table 2
Full equations for terms in Eq. (13) used to simultaneously estimate leaf and air temperatures.

Steady-state	Transient
$a_E = \frac{\overline{g}_{tR}\overline{e}_R + \overline{g}_{t0}\overline{e}_0 + \overline{g}_v e_s[\overline{T}_R]}{\overline{g}_{tR} + \overline{g}_{t0} + \overline{g}_v}$	$a_E = \frac{\frac{0.5t\overline{g}_v}{z_{LA}}\Delta_V[T_L^j]\Delta T_L}{1 + 0.5t\left(\frac{\overline{g}_{tR}}{z_R - z_i} + \frac{\overline{g}_{t0}}{z_i} + \frac{\overline{g}_v}{z_{LA}}\right)}$
$b_E = \frac{\Delta_V[\overline{T}_R]}{\overline{g}_{tR} + \overline{g}_{t0} + \overline{g}_v}$	$b_E = \frac{\frac{0.5t\overline{g}_v}{z_{LA}}\Delta_V[T_L^j]\Delta T_L}{1 + 0.5t\left(\frac{\overline{g}_{tR}}{z_R - z_i} + \frac{\overline{g}_{t0}}{z_i} + \frac{\overline{g}_v}{z_{LA}}\right)}$
$a_R = \varepsilon_s\sigma {a_A}^4$	$a_R = \varepsilon_s\sigma T_L^{j4}$
$b_R = 4\varepsilon_s\sigma({a_A}^3 b_A + \overline{T}_R{}^3)$	$b_R = \varepsilon_s\sigma 2T_L^{j3}$
$a_H = 0$	$a_H = c_p\overline{g}_{Ha}(T_L^j - a_A)$
$b_H = c_p\overline{g}_{Ha}$	$b_H c_p\overline{g}_{Ha}(0.5 - 0.5b_A)$
$a_L = \frac{\lambda\overline{g}_v}{\overline{p}_a}(e_s[\overline{T}_R] - a_e)$	$a_L = \frac{\lambda\overline{g}_v}{\overline{p}_a}(e_s[T_L^j] - a_e)$
$b_L = \frac{\lambda\overline{g}_v}{\overline{p}_a}(\Delta_V[\overline{T}_R] - b_E)$	$b_L = \frac{\lambda\overline{g}_v}{\overline{p}_a}(0.5\Delta_V[T_L^j] - b_E)$
$a_A = \frac{\overline{g}_{tR}\overline{T}_R + \overline{g}_{t0}\overline{T}_0}{\overline{g}_{tR} + \overline{g}_{t0}}$	$a_A = \frac{T_a^j + \frac{0.5}{m_a}\left\{\frac{\overline{g}_{tR}}{z_R - z_i}\overline{T}_R + \frac{\overline{g}_{t0}}{z_i}\overline{T}_0 + \frac{\overline{g}_{tR}}{z_{LA}}T_L^j + \frac{\lambda\overline{g}_v}{z_{LA}\overline{p}_a}(e_L^j + 0.5e_s[T_L^j]) - \frac{\lambda\overline{g}_v}{z_{LA}\overline{p}_a}a_E + \frac{\lambda\overline{g}_{t0}}{z_i\overline{p}_a}\overline{e}_0 - \frac{\lambda\overline{g}_{t0}}{z_i\overline{p}_a}a_E\right\}}{1 + \frac{0.5}{m_a}\left(\frac{\lambda\overline{g}_{t0}}{z_i\overline{p}_a} + \frac{\overline{g}_{t0}}{z_i} + \frac{\overline{g}_{Ha}}{z_{LA}}\right)}$
$b_A = \frac{\overline{g}_{Ha}}{\overline{g}_{tR} + \overline{g}_{t0}}$	$b_A = \frac{\frac{0.5}{m_a}\left\{0.5\frac{\overline{g}_{Ha}}{z_{LA}} + \frac{\lambda\overline{g}_v}{z_{LA}\overline{p}_a}(0.5\Delta_V[T_L^j] - b_E) + \frac{\lambda\overline{g}_{t0}}{z_i\overline{p}_a}b_E\right\}}{1 + \frac{0.5}{m_a}\left(\frac{\lambda\overline{g}_{t0}}{z_i\overline{p}_a} + \frac{\overline{g}_{t0}}{z_i} + \frac{\overline{g}_{Ha}}{z_{LA}}\right)}$, where $m_a = c_p\widehat{\rho}(1 - V_d)/tP_{AI}$

Terms are defined in Table 1. Overbars denote means during the time increment. Definitions for both steady-state and transient heat exchange are provided. Derivation of the equations is provided in Appendix A.

perscript j indicates the time at which temperature is determined and overbars indicate means during the time increment.

2.9. Within-canopy heat and vapour exchange

Under transient conditions, the approach described for soil can readily be extended to account for the exchange of heat between different layers of the canopy, with two notable exceptions. First, heat storage in the air is substantially lower than in the soil and prior to computing heat exchange between layers, air layers are merged when the total flux over the time increment exceeds heat capacity. Second, the latent and sensible heat fluxes from the leaf to the air are also considered

$$\overline{g}_{Ha}c_p\left(\overline{T}_L - \overline{T}_i\right) + \frac{\lambda\overline{g}_v}{\overline{p}_a}\left(\overline{e}_L - \overline{e}_a\right) + \overline{g}_i c_p\left(\overline{T}_{i+1} - \overline{T}_i\right) - \overline{g}_{i-1}c_p\left(\overline{T}_i - \overline{T}_{i-1}\right) = \frac{c_p\widehat{\rho}(1 - P_v)\left(T_i^{j+1} - T_i^j\right)(z_{i+1} - z_{i-1})}{2\Delta t} \quad (15)$$

where g_i is the molar conductance between canopy layers (7) and P_v is the fractional foliage volume given by $V_t[i]P_{AI}[i]/z_t[i]$, where $V_t[i]$ is the mean thickness of foliage and $z_t[i]$ the thickness of each canopy layer i.

The system of equations for each canopy layer can be combined with those for the soil layers to form a single set of equations. Assuming $\overline{T} = nT^{j+1} + (1 - n)T^j$, where n is a weighting factor in the range 0 to 1. Eqs. (14) and (15) can be re-arranged and solved for T^{j+1} by Gaussian elimination using the Thomas algorithm (Thomas, 1949), when boundary conditions are used to reduce the number of unknowns by two. The upper boundary condition is the conductance $\overline{g}_0$ between the top of the canopy and the air at reference height determined from (5). A boundary condition at the bottom of the soil profile is set by assuming that temperatures are stable and, in the absence of a user-provided value, equivalent to mean air temperature over the duration the model is run.

Vapour exchange can be handled in a similar way, expect that here, water exchange in the soil is user-specified, or in the steady-state mode, calculated using NicheMapR (see running the model) and the exchange between air layers is given by

$$\frac{\overline{g}_v}{\overline{p}_a}\left(\overline{e}_L - \overline{e}_a\right) + \frac{\overline{g}_i}{\overline{p}_a}\left(\overline{e}_{i+1} - \overline{e}_i\right) - \overline{g}_{i-1}c_p\left(\overline{e}_i - \overline{e}_{i-1}\right) = \frac{\widehat{\rho}(1 - P_v)\left(e_i^{j+1} - e_i^j\right)(z_{i+1} - z_{i-1})}{2\Delta t} \quad (1)$$

Again, the system of equations is solved by Gaussian elimination using the Thomas algorithm (see Appendix A).

3. Running the model

The model is split into two R packages. The package `microctools` contains a series of `worker` functions needed to run the model, such as those needed to compute conductance and radiation transmission. It also contains useful functions not directly needed to run the model, such as for estimating the diffuse fraction of total incoming solar radiation and converting between different humidity measures. The `microclimc` package contains the higher-level functions needed to compute individual elements of microclimate (for example leaf temperature), to run the model in its entirety over a single time increment (returning the full suite of microclimate variables for all layers in the canopy), or to run the model for a time-series to return temperature, humidity and wind speed at user-specified heights above or below ground. Package `microctools` is automatically installed when installing `microclimc` and is available on Github: https://github.com/ilyamaclean/microclimc.

There are two model run modes. Function `runmodel` runs the full model in transient mode, but in this mode, there are checks to establish whether conditions are steady state or transient, and the model automatically performs calculations accordingly. Function `runmodelS` runs the model in steady-state mode for cases in which predictions for a single height is desired. However, it is encouraged to conduct steady state modelling using the wrapper function `runwithNMR`, which invokes the `NicheMapR` package to calculate soil moisture from rainfall and

evapotranspiration. In alternative modes, soil moisture must be specified by the user.

Two sets of parameters are needed to drive the model: (1) vegetation parameters, describing canopy properties for multiple layers within the canopy and (2) soil parameters, enabling heat capacity and conductances within the soil to be calculated. However, a key goal in the development of this model is to enable estimates of microclimate with varying amounts of information available. The `microctools` package therefore includes functions that will reproduce reasonable approximations of soil properties simply by specifying a soil type and seasonal variation in and the vertical distribution of foliage and leaf angles from habitat types. Alternatively, where multi-layer information on foliage is available, such as might be derived using a plant canopy analyser or from a series of digital hemispherical photographs taken at different heights in the canopy (see e.g. Thimonier et al., 2010), these data can be used instead.

A similar ethos is used with regards to input weather data. The standard input is a data file of temperature, humidity, wind speed, air pressure, sky emissivity and incoming solar radiation, but where one or more of these variables are unavailable, we point the users to options for retrieving them. The R package `microclima' (Kearney et al., 2020; Maclean et al., 2019) contains functions for downloading, and interpolating to hourly, the required climate data from the NOAA-NCEP reanalyses programme (Kanamitsu et al., 2002). Similarly, the R-package 'mcera5' (Duffy, 2020) contains similar functions for retrieving data from the ECMWF ERA5 reanalysis programme (Hersbach, 2016). Full instructions for running the model are available as a vignette included with the package, provided in Appendix B. The model can be run in time-steps ranging from one second to daily, with the time-increment controlled by the climate forcing data provided.

4. Model validation

Both steady-state and transient modes of the model were validated using hourly empirical temperature measurements from four sites representing temperate deciduous and coniferous forests (Table 3; Lee et al., 1999; Munger and Hadley 2020; Templer et al., 2019; Teramoto et al., 2019)). Only validation data sampled according to best practices for micrometeorological observation (i.e. use of ultrafine-wire thermocouples; de Podesta et al., 2018; Rebmann et al., 2018) were used. Heights at which temperature was measured varied between sites (between 1.0 and 10.0 metres) but were always below the uppermost layers of the forest canopy; predictions were made for the same heights as measurements. The model was parameterized using biome-specific estimates of vegetation and soil profile parameters that are built into the package (see package details and vignette in Appendix B for details and the full list of parameters and default estimates).

We provided ERA5 hourly reanalysis data (Hersbach, 2016) as reference macroclimate and climate forcing to the microclimate model, corresponding to the times and points modelled. For the steady-state mode, daily resolution NCEP-DOE Reanalysis II precipitation estimates were provided for the soil moisture module (Kanamitsu et al., 2002). Because proper handling of snow cover and sub-freezing temperatures in the model is still under active development for the transient model, we constricted input data and predictions to only spring, summer and autumn months. For the purposes of this manuscript only air temperature predictions are validated (Figs. 1 and 2).

In the steady-state mode of the model, calculations are conducted simultaneously for all temporal timesteps, and therefore running the model for one year of data took an average of 5.28 s (on a single 2.2 GHz Intel i7 core with 4.0 GB of total memory). The transient mode, accessed via the function `runmodel`, must be run in sequence for each timestep, and so took an average of 194.9 s for the same time period. The steady-state and transient mode predicted below-canopy temperatures with similar accuracy (Mean absolute error 2.77 (transient) and 2.79 (steady-state); root mean square error 3.48 (both); 80.0% of variance explained (transient) and 79% (steady-state); Table 4). It should be noted that some of the error is likely due to errors associated with climate data used to drive the models.

Below-canopy temperatures were typically less variable than macroclimate temperatures, which was generally captured by the model in both of its modes. Both the steady-state and transient model underestimated forest temperature to a moderate degree (empirical SD: 5.93; steady-state estimate SD: 5.44; transient estimate SD: 4.67). At the Fuji Hokuroku and Hubbard Brook site there is also evidence of a fairly consistent over-estimation of temperatures. This may in part be attributable to altitudinal differences between validation sites and the coarse-resolution ERA5 data, which differ on average by 111 m from the mean elevation across the ~25-kilmetre ERA5 grid cells. For the purpose of reproducibility by users, and so as to provide a conservative estimate of model performance, we did not attempt to correct for these elevation differences.

5. Microclimate profiles

5.1. Thermal profiles

Typical profiles obtained by the model are shown in Figs. 3 and 4 and highlight the magnitude of differences in climatic conditions within the soil and above or below canopy. Here temperature and humidity profiles were predicted for a location in Cornwall, United Kingdom (50.2178°N, 5.32656°W) for a deciduous forest (Fig. 3) and short grassland (Fig. 4). In both instances, vegetation parameters were derived automatically by specifying a habitat type. In forest, under both dry and humid warm daytime conditions, air temperature averaged over 1 hour was predicted to have a maximum in mid-canopy. These findings are consistent with those of other studies (e.g. Finnigan, 2000), and indicative of a zone of high radiation absorption associated with high foliage density and reduced heat exchange with air above-canopy caused by greater distance and reduced wind speed. In contrast, leaf temperatures were

Table 3
Descriptions of sites and empirical temperature measurements used for model validation.

Name	Latitude, Longitude	Vegetation	Temperature sensor	Measurement height (m)	Time start	Time end
Borden Forest Research Station, Ontario, Canada	44°19′N, 79°56′W	Mixed hardwood/coniferous forest dominated by red maple and eastern white pine, 22 m canopy height	Aspirated copper–constantan thermocouples	1.7	1/04/1998	29/10/1998
Harvard Forest Hemlock Tower, Massachusetts, United States	42°32′N, 72°11′W	Hemlock-dominated temperate forest with mixed maple, oak, and pine, 23 m canopy height	Campbell Scientific CS215 sensor with aspirated radiation shield	1	4/04/2017	31/10/2017
Fuji Hokuroku Flux Observation Site, Yamanashi, Japan	35°27′N, 138°46′W	Deciduous and evergreen needleleaf forest, predominantly Japanese larch. 23 m canopy height	Vaisala HMP45A, platinum resistance thermometer	10	3/05/2019	30/09/2019
Hubbard Brook Experimental Forest	43°57′N, 71°42′W	Red maple-dominated mixed temperate forest, 22 m canopy height	Campbell Scientific CS215 sensor with aspirated radiation shield	6	1/04/2013	30/09/2013

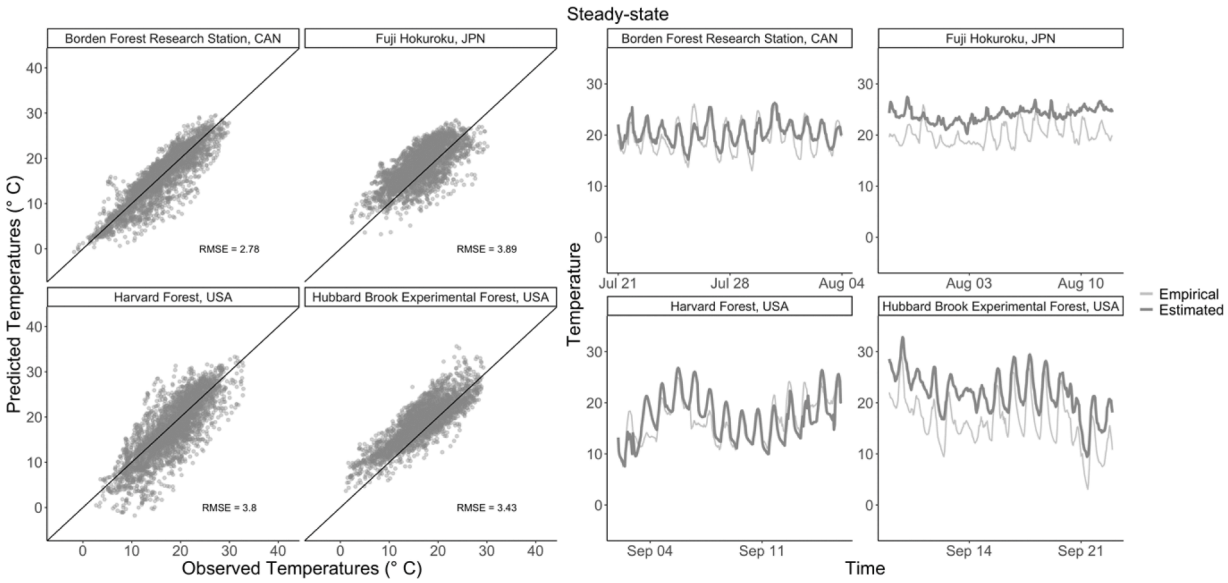

Fig. 1. Steady-state model predictions of temperature plotted across empirical measurements at four forested sites. Measurements were taken at heights ranging from 1.0 m to 10.0, but all below the uppermost layers of canopy. Both thermal measurements and predictions were taken at hourly time-steps for 5–7 months per site, and here subsets of time series are plotted to demonstrate diel variability.

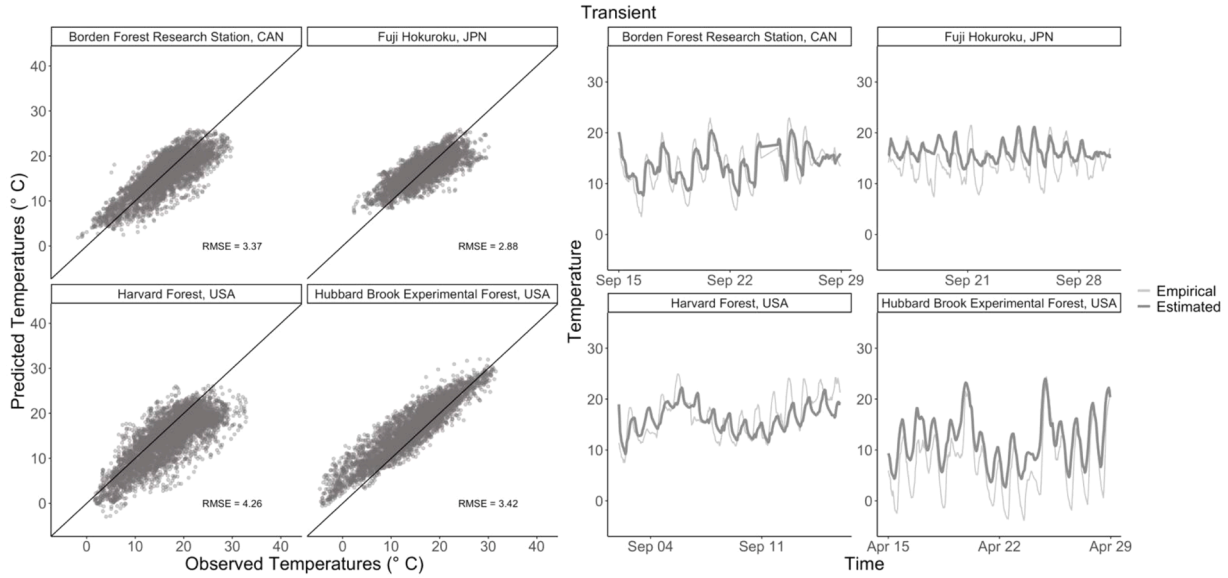

Fig. 2. Transient model predictions of temperature plotted across empirical measurements at four forested sites. Transient predictions had moderately lower error than steady-state predictions (Fig. 1), although the model did not accurately predict temperatures near freezing.

Table 4
Microclimate model average performance in steady-state and transient modes.

Variable	Steady-State	Transient
Avg. run time (1 year time series)	5.28 s	187.80 s
MAE	3.3	2.77
RMSE	4.15	3.48
r^2	0.803	0.8

Mean absolute error, root mean square error, and Pearson's correlation coefficients reported are relative to the empirical temperature measurements.

predicted to be highest near the top of the canopy, where self-shading is lowest. At night, leaf temperatures are lowest near the top of the canopy, particularly under clear-sky conditions. Here a lower proportion of the radiation emitted by a leaf would be expected to be absorbed and re-emitted by the canopy. In contrast, differences in canopy air temperatures were predicted to be modest. The cooling effect of leaves is offset by greater heat exchange with air above the canopy. The relative humidity profile reflects three factors. On the one hand, relative humidity would be expected to be lowest where temperatures are higher, as for a given vapour pressure relative humidity is primarily a function of temperature. However, evapotranspiration from leaves and vapour exchange with air above the canopy are also important. Despite limitations in the extent to which *K*-theory accurately captures canopy turbulence, the predicted wind profiles are remarkably similar to empirically-derived profiles reported in other studies (e.g. Raupach and Thom, 1981).

In the grassland, particularly in sunny conditions, air temperature decreases with height above-canopy and is highest at points near the top of the canopy. Temperatures in the soil decrease with depth. At night, under cold, clear-sky conditions when air temperature is lower than that

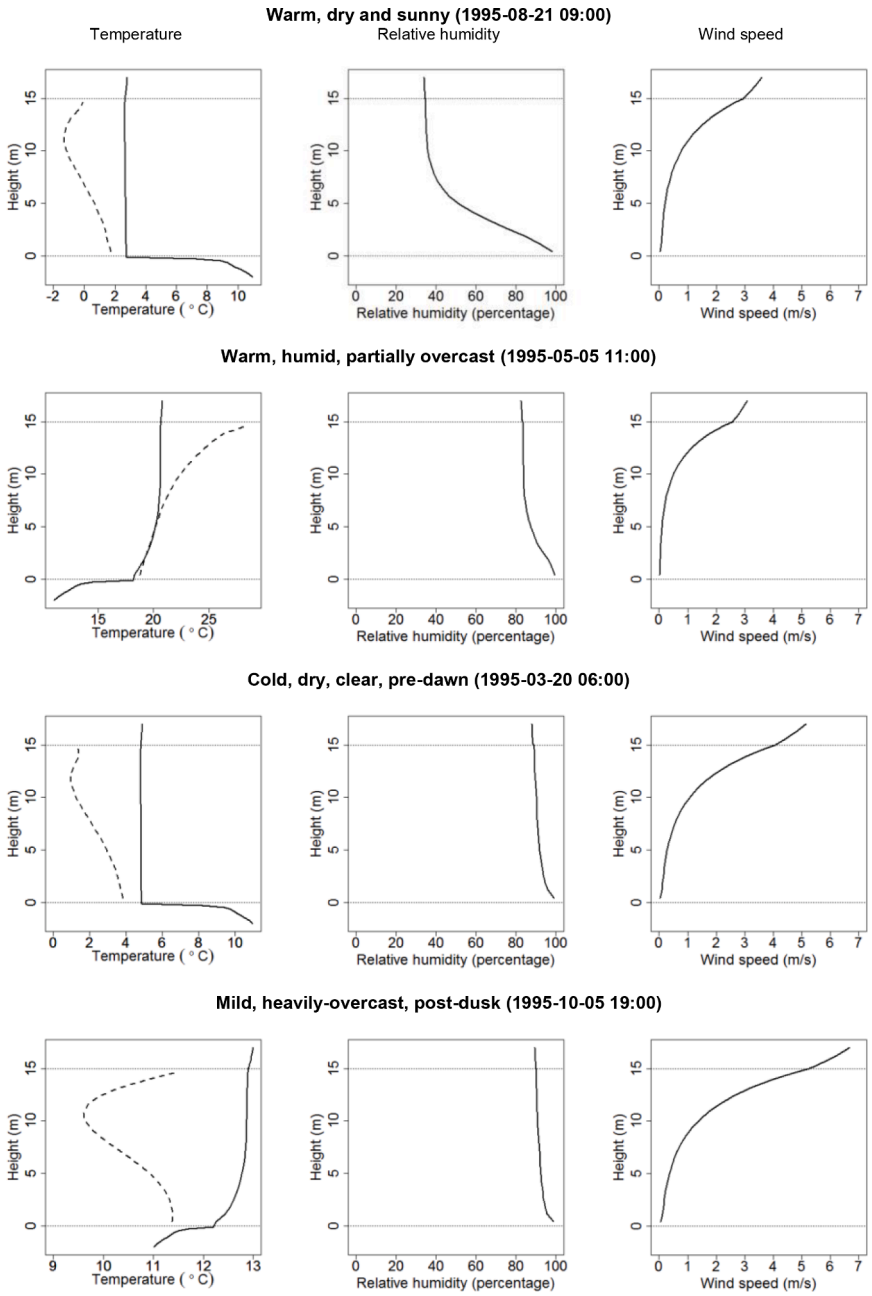

Fig 3. Modelled temperature (left), relative humidity (middle) and wind profiles (right) above, below and within a 15 m tall deciduous forest canopy on four days with contrasting weather conditions. Dotted lines in temperature profiles represent leaf temperatures, solid lines air temperature.

of the deepest soil layer, the profile is reversed. Under overcast conditions, when air temperatures are similar to ground temperatures, variation in temperature with height is minimal, though there is a distinct zone close to the soil surface where temperatures are lower. Leaf temperature profiles are broadly similar to air temperature profiles within the canopy. As with deciduous forest, relative humidity profiles partially reflect the temperature profiles, being lowest where temperatures are higher. However, is noticeable that during dry sunny conditions relative humidity is highest within the vegetation itself, despite warmer temperatures, reflecting the zone of evapotranspiration. Wind profiles are typical of those empirically observed (Campbell and Norman, 2012), and, though partially affected by diabatic turbulence, are broadly consistent irrespective of conditions.

6. Concluding remarks

Our model, written for the R programming environment, complements existing R packages for modelling microclimate (Kearney and Porter, 2017; Maclean et al., 2019), but extends the utility of these packages by enabling ecologists to predict adequately the microclimate above, within, and below dense canopies, such as those of forests. Since many organisms live in forest environments, this is likely to be particularly useful. A key goal in developing our model was to enable estimates of microclimate with varying amounts of information available. In consequence, default parameters drawn from literature are provided for broad habitat and soil types, but in circumstances where more detailed site-specific information, this can be readily incorporated. Estimates of snow cover and its effects on temperature can be accounted for by invoking the snow subroutine within the `NicheMapR` package, which builds nodes of snow above the surface conditional on the amount of

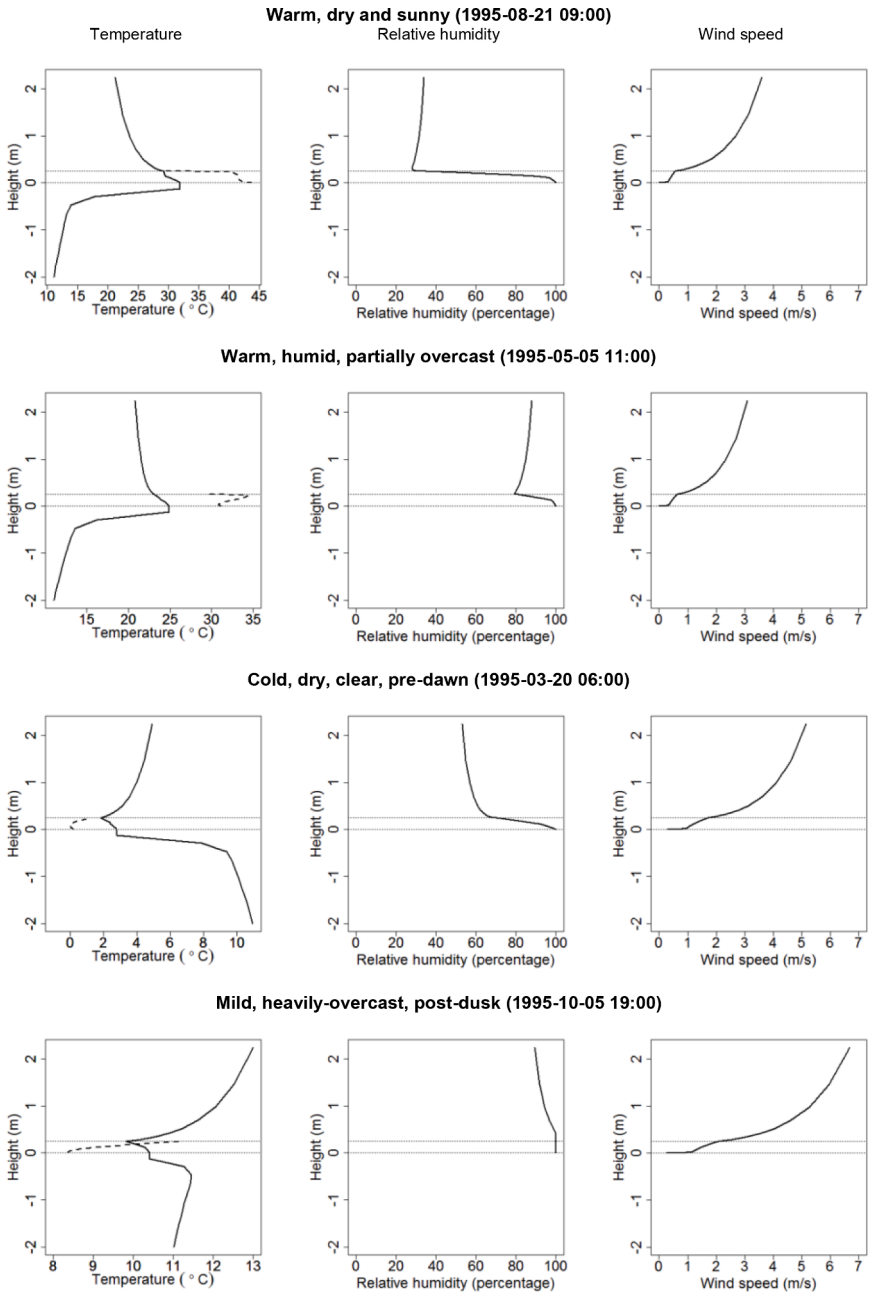

Fig 4. Modelled temperature (left), relative humidity (middle) and wind profiles (right) above, below and within a 25 cm height grassland on four days with contrasting weather conditions. Dotted lines in temperature profiles represent leaf temperatures, solid lines air temperature.

precipitation, and thereby influencing albedo and surface-air heat exchange. Accounting for snow would be especially valuable for improved predictions near freezing, a current limitation of our model. Predictions of below-canopy soil temperatures are currently provided by the model, yet these are primarily to estimate heat exchange with the air. Accurate soil temperature predictions are contingent upon capturing dynamic soil moisture, which in the steady-state mode can be achieved via integration with `NicheMapR`.

Time series of sub-canopy temperatures from four forest locations globally are used to test the model. The results indicate that temperatures can be estimate with a moderate degree of accuracy. A degree of error is to be expected, however, as the climate forcing datasets used to drive the model are themselves imperfect and used we used default vegetation parameters associated with the broad habitat types of these sites rather than quantifying vegetation structure in situ. Improvements in model fit would be expected with finer-tuning of model parameters to account for local conditions and by correcting the climate forcing data, for example by accounting for elevation effects (see e.g. Maclean et al., 2019). Nevertheless, even without doing so, the mean error of temperature measurements is only in the order of 2.5–3 °C.

Though there are still uncertainties in understanding of the microclimatic processes operating below canopy, many of the fundamental principles of microclimate modelling have been resolved decades. However, few of these insights have diffused into the field of ecology and the lack of integration between ecology and micrometeorology is perhaps one of the most remarkable examples of a disciplinary division. While many of the principles of microclimate modelling were resolved decades ago, in the very situations in which such models are much needed, they are rarely utilised. Here we utilised principles of environmental physics to provide a step forward in bridging this gap.

Credit author statement

IMDM developed and coded the model and wrote the manuscript. DHK performed model validation and verification and contributed to writing the manuscript and supporting information.

Declaration of Competing Interest

On behalf of both authors, I hereby confirm no competing interests.

Acknowledgments

The work was supported by the Met Office Hadley Centre Climate Programme (HCCP) funded by BEIS and Defra through collaboration with Dr Deborah Hemming, who leads HCCP work on UK pest risk with Defra's Animal and Plant Health Team. Additional support was provided by the European Regional Development Fund Agri-tech Cornwall Programme. DK was supported by the National Science Foundation Graduate Research Fellowship Program (No. 2019277511). We thank anonymous referees for helpful comments and Katie Thurston for proofreading the manuscript.

Supplementary materials

Supplementary material associated with this article can be found, in the online version, at doi:10.1016/j.ecolmodel.2021.109567.

References

Ali, H.B., Bournet, P.-E., Cannavo, P., Chantoiseau, E., 2018. Development of a CFD crop submodel for simulating microclimate and transpiration of ornamental plants grown in a greenhouse under water restriction. Comput. Electron. Agric. 149, 26–40.
Bache, D., 1986. Momentum transfer to plant canopies: influence of structure and variable drag. Atmos. Environ. 20, 1369–1378.
Bailey, B.N., Stoll, R., Pardyjak, E.R., Miller, N.E., 2016. A new three-dimensional energy balance model for complex plant canopy geometries: model development and improved validation strategies. Agric. For. Meteorol. 218, 146–160.
Baker, C., 1980. Some Problems in Using Meteorological Data to Forecast the Timing of Insect Life Cycles 1: problčmes rencontrés dans L'utilisation des données météorologiques pour prévoir le cycle évolutif des insectes. EPPO Bull. 10, 83–91.
Baldocchi, D., Meyers, T., 1998. On using eco-physiological, micrometeorological and biogeochemical theory to evaluate carbon dioxide, water vapor and trace gas fluxes over vegetation: a perspective. Agric. For. Meteorol. 90, 1–25.
Bennie, J., Huntley, B., Wiltshire, A., Hill, M.O., Baxter, R., 2008. Slope, aspect and climate: spatially explicit and implicit models of topographic microclimate in chalk grassland. Ecol. Modell. 216, 47–59.
Bramer, I., Anderson, B.J., Bennie, J., Bladon, A.J., De Frenne, P., Hemming, D., Hill, R. A., Kearney, M.R., Körner, C., Korstjens, A.H., 2018. Advances in monitoring and modelling climate at ecologically relevant scales. Adv. Ecol. Res. 58, 101–161.
Bruse, M., 2014. ENVI-Met 4.
Buckley, L.B., Cannistra, A.F., John, A., 2018. Leveraging organismal biology to forecast the effects of climate change. Integr. Comp. Biol. 58, 38–51.
Campbell, G., 1990. Derivation of an angle density function for canopies with ellipsoidal leaf angle distributions. Agric. For. Meteorol. 49, 173–176.
Campbell, G.S., 1985. Soil Physics With BASIC: Transport Models For Soil-Plant Systems. Elsevier.
Campbell, G.S., 1986. Extinction coefficients for radiation in plant canopies calculated using an ellipsoidal inclination angle distribution. Agric. For. Meteorol. 36, 317–321.
Campbell, G.S., Norman, J., 2012. An Introduction to Environmental Biophysics. Springer Science & Business Media.
Cionco, R.M., 1972. A wind-profile index for canopy flow. Boundary Layer Meteorol. 3, 255–263.
Curtis, E.M., Knight, C.A., Leigh, A., 2019. Intracanopy adjustment of leaf-level thermal tolerance is associated with microclimatic variation across the canopy of a desert tree (Acacia papyrocarpa). Oecologia 189, 37–46.
de Podesta, M., Bell, S., Underwood, R., 2018. Air temperature sensors: dependence of radiative errors on sensor diameter in precision metrology and meteorology. Metrologia 55, 229–244.
Dolman, A., Wallace, J., 1991. Lagrangian and K-theory approaches in modelling evaporation from sparse canopies. Q. J. R. Meteorolog. Soc. 117, 1325–1340.
Duffy, J.P., 2020. R Package mcera5. Tools to Acquire and Process ERA5 Data for Use in Microclimate Modelling. Available. https://github.com/everydayduffy/mcera5.
Evans, M.R., 2012. Modelling ecological systems in a changing world. Philos. Transac. R. Soc. B: Biol. Sci. 367, 181–190.
Fick, S.E., Hijmans, R.J., 2017. WorldClim 2: new 1-km spatial resolution climate surfaces for global land areas. Int. J. Climatol. 37, 4302–4315.
Finnigan, J., 2000. Turbulence in plant canopies. Annu Rev Fluid Mech 32, 519–571.
Gardner, A.S., Maclean, I.M., Gaston, K.J., 2020. A new system to classify global climate zones based on plant physiology and using high temporal resolution climate data. J. Biogeogr.
Gardner, T.A., Barlow, J., Chazdon, R., Ewers, R.M., Harvey, C.A., Peres, C.A., Sodhi, N. S., 2009. Prospects for tropical forest biodiversity in a human-modified world. Ecol. Lett. 12, 561–582.
Geiger, R., 1954. Klassifikation der klimate nach W. Köppen. Landolt-Börnstein–Zahlenwerte und Funktionen aus Physik, Chemie, Astronomie, Geophysik und Technik 3, 603–607.
Goudriaan, J., 1977. Crop micrometeorology: a Simulation Study. Pudoc.
Greiser, C., Meineri, E., Luoto, M., Ehrlén, J., Hylander, K., 2018. Monthly microclimate models in a managed boreal forest landscape. Agric. For. Meteorol. 250, 147–158.
Hersbach, H., 2016. The ERA5 Atmospheric Reanalysis, AGU fall meeting abstracts.
Ingenhousz, J., 1779. Experiments Upon vegetables: Discovering Their Great Power of Purifying the Common Air in the sun-shine, and of Injuring It in the Shade and At night. To which is joined, a New Method of Examining the Accurate Degree of Salubrity of the Atmosphere. Printed by P. Elmsly and H. Payne.
Inoue, E., 1963. On the Turbulent Structure of Airflow within. Journal of the Meteorological Society of Japan. Ser. II 41, 317–326.
Jarvis, P.G., McNaughton, K.G., 1986. Stomatal control of transpiration: scaling up from leaf to region. Adv. Ecol. Res. 15, 1–49.
Kanamitsu, M., Ebisuzaki, W., Woollen, J., Yang, S.-K., Hnilo, J., Fiorino, M., Potter, G., 2002. Ncep–doe amip-ii reanalysis (r-2). Bull. Am. Meteorol. Soc. 83, 1631–1644.
Katul, G.G., Albertson, J.D., 1999. Modeling CO2 sources, sinks, and fluxes within a forest canopy. J. Geophys. Res.: Atmos. 104, 6081–6091.
Kearney, M.R., Gillingham, P.K., Bramer, I., Duffy, J.P., Maclean, I.M., 2020. A method for computing hourly, historical, terrain-corrected microclimate anywhere on Earth. Methods Ecol. Evol. 11, 38–43.
Kearney, M.R., Porter, W.P., 2017. NicheMapR–an R package for biophysical modelling: the microclimate model. Ecography 40, 664–674.
Kelliher, F.M., Leuning, R., Raupach, M., Schulze, E.-.D., 1995. Maximum conductances for evaporation from global vegetation types. Agric. For. Meteorol. 73, 1–16.
Köppen, W., 1884. Die Wärmezonen der Erde, nach der Dauer der heissen, gemässigten und kalten Zeit und nach der Wirkung der Wärme auf die organische Welt betrachtet. Meteorol. Z. 1, 5–226.
Körner, C., 1995. Leaf Diffusive Conductances in the Major Vegetation Types of the globe, Ecophysiology of Photosynthesis. Springer, pp. 463–490.
Kumarathunge, D.P., Medlyn, B.E., Drake, J.E., Tjoelker, M.G., Aspinwall, M.J., Battaglia, M., Cano, F.J., Carter, K.R., Cavaleri, M.A., Cernusak, L.A., 2019. Acclimation and adaptation components of the temperature dependence of plant photosynthesis at the global scale. New Phytol. 222, 768–784.
Lee, X., Fuentes, J.D., Staebler, R.M., Neumann, H.H., 1999. Long-term observation of the atmospheric exchange of CO2 with a temperate deciduous forest in southern Ontario, Canada. J. Geophys. Res.: Atmos. 104, 15975–15984.
Lembrechts, J.J., Lenoir, J., 2019. Microclimatic Conditions Anywhere at Any time! Global Change Biology.
Lembrechts, J.J., Nijs, I., Lenoir, J., 2019. Incorporating microclimate into species distribution models. Ecography 42, 1267–1279.
Lenoir, J., Hattab, T., Pierre, G., 2017. Climatic microrefugia under anthropogenic climate change: implications for species redistribution. Ecography 40, 253–266.
Lowman, M., Nadkarni, N., Mitchell, D., 1996. Forest canopies. Biol. J. Linn. Soc. 59, 217.
Maclean, I.M., 2020. Predicting future climate at high spatial and temporal resolution. Glob Chang Biol 26, 1003–1011.
Maclean, I.M., Mosedale, J.R., Bennie, J.J., 2019. Microclima: an R package for modelling meso-and microclimate. Methods Ecol. Evol. 10, 280–290.
Maclean, I.M., Suggitt, A.J., Wilson, R.J., Duffy, J.P., Bennie, J.J., 2017. Fine-scale climate change: modelling spatial variation in biologically meaningful rates of warming. Glob. Chang. Biol. 23, 256–268.
McNaughton, K., Van den Hurk, B., 1995. A 'Lagrangian'revision of the resistors in the two-layer model for calculating the energy budget of a plant canopy. Boundary Layer Meteorol. 74, 261–288.
Meineri, E., Hylander, K., 2017. Fine-grain, large-domain climate models based on climate station and comprehensive topographic information improve microrefugia detection. Ecography 40, 1003–1013.
Michaletz, S.T., Weiser, M.D., McDowell, N.G., Zhou, J., Kaspari, M., Helliker, B.R., Enquist, B.J., 2016. The energetic and carbon economic origins of leaf thermoregulation. Nat Plants 2, 1–9.
Mitchell, J.W., 1976. Heat transfer from spheres and other animal forms. Biophys. J. 16, 561–569.
Monin, A.S., Obukhov, A.M., 1954. Basic laws of turbulent mixing in the surface layer of the atmosphere. Contrib. Geophys. Inst. Acad. Sci. USSR 151, e187.
Monteith, J., Unsworth, M., 2013. Principles of Environmental physics: plants, animals, and the Atmosphere. Academic Press.
Monteith, J.L., 1965. Evaporation and environment. Symp. Soc. Exp. Biol. 19, 205–224.
Munger, W., Hadley, J., 2020. Net Carbon Exchange of an Old-Growth Hemlock Forest at Harvard Forest HEM Tower since 2000. Harvard Forest Data Archive HF103.
Nabi, I., 1985. On the Tendencies of Motion. In: Levins, R., Lewontin, R. (Eds.), The Dialectical Biologist. Harvard University Press, Cambridge, MA, pp. 124–126.
Nakamura, A., Kitching, R.L., Cao, M., Creedy, T.J., Fayle, T.M., Freiberg, M., Hewitt, C., Itioka, T., Koh, L.P., Ma, K., 2017. Forests and their canopies: achievements and horizons in canopy science. Trends Ecol. Evol. (Amst.) 32, 438–451.
Penman, H.L., 1948. Natural evaporation from open water, bare soil and grass. Proc. R. Soc. Lond. Ser A. Math. Phys. Sci. 193, 120–145.
Perez, T.M., Feeley, K.J., 2020. Photosynthetic heat tolerances and extreme leaf temperatures. Funct Ecol 00, 1–10.

Porter, W., Mitchell, J., Beckman, W., DeWitt, C., 1973. Behavioral implications of mechanistic ecology. Oecologia 13, 1–54.
Potter, K.A., Arthur Woods, H., Pincebourde, S., 2013. Microclimatic challenges in global change biology. Glob Chang Biol 19, 2932–2939.
Prandtl, L., 1925. Bericht über die Entstehung der Turbulenz. Z. Angew. Math. Mech 5, 136–139.
Raupach, M., 1989. Applying Lagrangian fluid mechanics to infer scalar source distributions from concentration profiles in plant canopies. Agric. For. Meteorol. 47, 85–108.
Raupach, M., Thom, A.S., 1981. Turbulence in and above plant canopies. Annu. Rev. Fluid Mech. 13, 97–129.
Rebmann, C., Aubinet, M., Schmid, H., Arriga, N., Aurela, M., Burba, G., Clement, R., De Ligne, A., Fratini, G., Gielen, B., 2018. ICOS eddy covariance flux-station site setup: a review.
Richardson, L., 1922. Weather Prediction By Numerical Process (Cambridge U. Press). Dover Publications edition, New York, 1965.
Shaw, R.H., Pereira, A., 1982. Aerodynamic roughness of a plant canopy: a numerical experiment. Agric. Meteorol. 26, 51–65.
Suggitt, A.J., Gillingham, P.K., Hill, J.K., Huntley, B., Kunin, W.E., Roy, D.B., Thomas, C. D., 2011. Habitat microclimates drive fine-scale variation in extreme temperatures. Oikos 120, 1–8.
Suggitt, A.J., Wilson, R.J., Isaac, N.J., Beale, C.M., Auffret, A.G., August, T., Bennie, J.J., Crick, H.Q., Duffield, S., Fox, R., 2018. Extinction risk from climate change is reduced by microclimatic buffering. Nat. Clim. Chang. 8, 713.
Templer, P., Sanders-DeMott, R., Juice, S., Bowles, F., Sofen, L., Harrison, J., 2019. Climate Change Across Seasons Experiment (CCASE) at the Hubbard Brook Experimental Forest: soil and Air Temperature. Environ. Data Initiative. https://doi.org/10.6073/PASTA/C6A9AC6C5CBC05888170902B8AF54869 v3.
Teramoto, M., Liang, N., Takahashi, Y., Zeng, J., Saigusa, N., Ide, R., Zhao, X., 2019. Enhanced understory carbon flux components and robustness of net CO2 exchange after thinning in a larch forest in central Japan. Agric. For. Meteorol. 274, 106–117.
Thimonier, A., Sedivy, I., Schleppi, P., 2010. Estimating leaf area index in different types of mature forest stands in Switzerland: a comparison of methods. Eur. J. For. Res. 129, 543–562.
Thomas, L., 1949. Elliptic Problems in Linear Differential Equations Over a network: Watson scientific Computing Laboratory. Columbia Univ., NY.
Waggoner, P.E., Furnival, G., Reifsnyder, W., 1969. Simulation of the microclimate in a forest. For. Sci. 15, 37–45.